Article

Journal of the Brazilian Chemical Society

https://dx.doi.org/10.21577/0103-5053.20240007

J. Braz. Chem. Soc. **2024**, *35*, 7, e-20240007, 1-10

$PdAg/CoFe_2O_4$ Bimetallic Catalyst with High Selectivity for Glyceraldehyde in Glycerol Selective Oxidation Reaction

Milton S. Falcão, [a] ***Edmilson M. de Moura,*** [*,b] ***Jean C. S. Costa,*** [b] ***Antonio F. A. A. Melo,*** [c] ***Gilvan M. Paz,*** [c] ***Ronaldo F. do Nascimento,*** [d] ***Hélio O. do Nascimento*** [d] ***and Luciano A. Montoro*** [e]

[a]*Departamento de Ensino, Instituto Federal de Educação, Ciência e Tecnologia do Maranhão, 65365-000 Zé Doca-MA, Brazil*

[b]*Departamento de Química, Universidade Federal do Piauí, 64049-550 Teresina-PI, Brazil*

[c]*Departamento de Química, Instituto Federal de Educação, Ciência e Tecnologia do Piauí, 64000-5040 Teresina-PI, Brazil*

[d]*Departamento de Química Analítica e Físico-Química, Universidade Federal do Ceará, 60455-760 Fortaleza-CE, Brazil*

[e]*Departamento de Química, Universidade Federal de Minas Gerais, 31270-901 Belo Horizonte-MG, Brazil*

The catalytic oxidation of glycerol was investigated in assays with palladium-silver bimetallic nanoparticles (Pd-Ag) immobilized on cobalt ferrite ($CoFe_2O_4$). Bimetallic nanoparticles were prepared by the galvanic replacement method, immobilized on $CoFe_2O_4$ by wet impregnation. Bimetallic Pd-Ag nanoparticles with 35 wt.% Pd content effectively catalyzed the selective oxidation reaction of glycerol to glyceraldehyde. Catalytic oxidation was carried out at 60-80 °C for 2-4 h in an aqueous NaOH solution (NaOH:glycerol ratio = 4 mol:mol) under O_2 pressure of 4 bar; the selectivity of glyceraldehyde reached 99.35% and the conversion of glycerol of 49.07% at a temperature of 60 °C and a reaction time of 2 h. Glyceric acid and traces of tartronic acid and mesoxalic acid were also detected. The catalyst was also very stable, showing activity up to 4 runs without significant loss of activity and selectivity.

Keywords: glycerol, selective oxidation, glyceraldehyde, bimetallic Ag-Pd, magnetic support

Introduction

Reactions involving organic compounds such as hydrocarbons,[1] alcohols,[2-5] among others, have been widely used, as options, for the degradation of industrial waste substances, pollutants, and drugs, in the production of raw materials for various industrial sectors and as a route for the scheme of compounds with high added value[4,6-9], for example, the synthesis of glyceric acid from glycerol (GLY) derived from the biofuels industry.[10]

The selective oxidation of alcohol has been highlighted[1,11] in recent years due to its environmental and economic importance. As a result, new research aimed at increasing the viability of oxidation processes is being developed in academia, which mainly points to knowledge of the reaction mechanism[12,13] and the search for new catalysts with greater efficiency,[14,15] low cost and greener.[16]

Oxidation reactions can occur through different routes, such as enzymatic,[17] electrocatalytic,[18] photocatalytic[19,20] or by selective oxidation.[4,21] The use of metallic nanoparticles as catalysts for the selective oxidation of benzyl alcohol shows good results.[22] Melo *et al.*[23] used gold and palladium nanoparticles supported by strontium carbonate ($Au-Pd/SrCO_3$) in selective oxidation tests of benzyl alcohol and observed an average conversion of 95% under optimized reaction conditions with about 83% selectivity for benzyl benzoate for 6 runs without significant loss of catalytic performance. It is also observed that catalysts based on metallic nanoparticles, when supported

*e-mail: mmoura@ufpi.edu.br
Editor handled this article: Célia M. Ronconi (Associate)

on oxides, reduce the cost, increase activity and are more easily recovered for reuse. Pereira *et al.*[24] demonstrated that gold nanoparticles supported on surface $CoFe_2O_4$ enriched with $Sr(OH)_2$ showed significant control of the selectivity of the oxidation reaction from benzyl alcohol to benzaldehyde without the need to add a base to alkalize the reaction medium.

Just like benzyl alcohol, nanoparticles of noble metals such as gold, silver, palladium and platinum have pronounced activity for the selective oxidation of other alcohols such as 1,2 propanediol and GLY.[2,25-27] GLY is a trialcohol whose oxidation products, such as glyceraldehyde (GALD) and glyceric acid (GLYA), have a high added commercial value (Figure 1), which creates the need to use a catalyst that, more than presenting a high conversion power, is very selective for a given product, otherwise the cost of purifying the products obtained may increase the process so much that it becomes unfeasible to use it. Thus, there is a need to choose a selective catalyst for a specific product and simplify and make the purification step less expensive. Typically, the oxidation of GLY would occur through the reaction pathway described in Figure 1 with the formation of GALD by the reaction of a primary hydroxyl; GLAD undergoes new oxidation, this time, in the carbonyl group that leads to the formation of GLYA, which in turn undergoes oxidation of the terminal hydroxyl and then of the secondary hydroxyl with the formation of tartronic acid (TART) and mesoxalic acid (MESO), respectively. Another possible route considers the formation of dihydroxyacetone (DHA) from the oxidation of the central hydroxyl and this in turn can undergo oxidation with formation of hydroxypyruvic acid (HYP).[28]

Hirasawa *et al.*[29] in their tests using bimetallic nanoparticles based on silver and palladium supported on activated carbon (carbon black) as a catalyst, observed high selectivity of the reaction process for the formation of DHA. The basicity of the support combined with the size of metallic nanoparticles was studied by Pakrieva *et al.*[30], who observed high selectivity for GLYA (38-72%) using pure oxides (TiO_2, CeO_2, La_2O_3 and MgO) or oxides modified with titanium oxide (CeO_2/TiO_2, La_2O_3/TiO_2 and MgO/TiO_2). The use of bimetallic particles as a catalyst for the oxidation of glycerol allows for an increase in the conversion and selectivity of the catalyst and this activity can even be improved by the use of appropriate support. Dodekatos *et al.*[31] studied gold nanoparticles immobilized on the surface of MgO and γ-Al_2O_3 and obtained a yield of 98% in 3 h of reaction with a small difference in selectivity for GLYA and tartronic acid using monometallic catalysts. For bimetallic catalysts (gold and palladium) a pronounced difference in selectivity can be observed, especially for GLYA.

The composition of the support and of the metals that form the catalyst, as well as the synthesis method, influence the performance during the reaction, in terms of conversion and selectivity, in addition to facilitating its reuse; considering this evidence, the proposed study aims to evaluate the catalytic potential of bimetallic nanoparticles based on silver and palladium produced by galvanic substitution and supported on cobalt ferrite in reactions of selective oxidation of glycerol.

Experimental

Materials and methods

Iron(III) chloride hexahydrate ($FeCl_3.6H_2O$, purity 98%), cobalt(II) chloride hexahydrate ($CoCl_2.6H_2O$, purity 98%) and ammonium hydroxide solution (NH_4OH, 28-30%) were from ACS reagent (Rio de Janeiro, Brazil). Sodium tetrachloropalladate(II) (Na_2PdCl_4, purity > 99.99%), silver nitrate ($AgNO_3$, purity ≥ 99.00%), polyvinylpyrrolidone (PVP) (molecular weight = 55,000), sodium borohydride ($NaBH_4$, purity > 98.0%) were from Aldrich (São Paulo, Brazil). $NaBH_4$ (0.025 mol L^{-1}) was freshly prepared. GLY, GLYA and all the intermediates were from Sigma-Aldrich Brasil Ltda, São Paulo-SP, Brazil. Deionized water (Milli-Q purified, São Paulo, Brazil) was used in all the experiments.

Synthesis PdAg/$CoFe_2O_4$

The nanoparticles of the magnetic support of cobalt ferrite (CF) were synthesized by the co-precipitation method according to Falcão *et al.*[32] The bimetallic particles were synthesized by galvanic substitution in a method adapted from Chen *et al.*[11] and the functionalization process with bimetallic nanoparticles occurred by wet impregnation

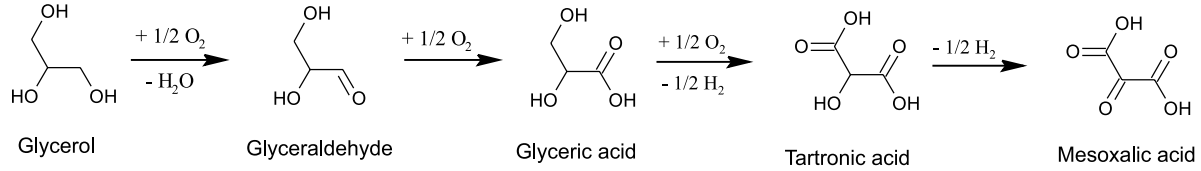

Figure 1. Simplified scheme of reaction pathways for selective oxidation of glycerol.[28]

in an adapted method.[33-36] Three different palladium-silver ratios were synthesized (Pd/(Pd-Ag) = 0.20, 0.40 and 0.80) and considered in this study in order to define their effect on the catalytic performance of the produced composite. Cobalt ferrite magnetic nanoparticles were prepared by a co-precipitation method. An aqueous solution of $FeCl_3.6H_2O$ (10 mL, 1.65 mol L^{-1}) was mixed with an aqueous solution of $CoCl_2.6H_2O$ (5 mL, 1.65 mol L^{-1}) dissolved in 2 mol L^{-1} HCl. The solution prepared was added to 250 mL of ammonium hydroxide aqueous solution (0.7 mol L^{-1}) and mechanically stirred at 95 °C for 120 min in a reflux system. The black precipitate formed was cooled down to room temperature, collected with a permanent magnet and washed 3 times with distilled water and once with acetone. The solid was dried in a muffle furnace for 6 h at 120 °C and, then, calcined in atmospheric air for 2 h at 600 °C.

Silver nanoparticles were synthesized by the *ex situ* method in which an aqueous solution of $AgNO_3$ (0.050 mol L^{-1}) containing 2.0% PVP was heated at 60 °C under magnetic stirring for 3 h; After this step, a freshly prepared $NaBH_4$ aqueous solution (0.025 mol L^{-1}) was added to reduce the metal, maintaining the magnetic stirring. The solution turned yellow instantly and the stirring continued for an additional 30 min. Next, a solution of 0.002 mol L^{-1} Na_2PdCl_4 was added dropwise to carry out the galvanic substitution with the consequent synthesis of silver-palladium bimetallic particles in different proportions (Pd/(Pd-Ag) = 0.20, 0.40 and 0.80). In the next step (30 min later), 100 mg CF were added and kept under magnetic stirring for 12 h. The catalyst produced was named CAP.

The catalyst was synthesized to contain 1.00 wt.% palladium silver nanoparticles (NPs) separated using a neodymium magnet and washed three times with water (50 mL) before being placed in an oven at 120 °C for 12 h; finally, the materials were calcined at 600 °C for 2 h in a muffle and stored in an amber flask.

After each use, the catalyst was removed from the reaction medium by magnetization, washed with distilled water at room temperature and dried in an oven at 120 °C for 12 h, then, the dried material was calcined in a muffle furnace at 600 °C for 2 h and reused.

Characterizations

The magnetic characterization was performed by using an EZ9 MicroSense (Porto Alegre, Brazil) vibrating sample magnetometer (VSM) at room temperature with a magnetic field cycled between –22 and +22 kOe. X-ray fluorescence analysis (XRF) was performed in energy-dispersive X-ray fluorescence spectrometer EPSILON 3 XL equipment (Recife, Brazil) operating with a metal-ceramic X-ray tube and a maximum voltage of 50 kV. The UV-Vis spectroscopy was carried out with GENESYS 10S UV-Vis v4.006 spectrophotometer (Teresina, Brazil) operating in the scanning range of 200 to 800 nm. Quartz cuvettes with a 1 cm optical path were used, and the samples were dispersed in water by an ultrasonic bath. Thermogravimetric (TGA) measurements were performed on a DTG-60/DTG-60A Shimadzu equipment (Teresina, Brazil) TG/DTA (differential thermal analysis) simultaneous measuring instrument. The X-ray diffractograms (XRD) were obtained using Bruker D8 Advance equipment (Teresina, Brazil) using monochromatic Cu Kα radiation (λ = 1.54056 Å) and graphite monochromator. The voltage of the copper emission tube was 40 kV and the filament current was 40 mA, at a 2θ range from 5° to 90° with a 0.02° step size and measuring time of 5 s *per* step. Transmission electron microscopy (TEM) images were obtained with a MET-MORGANI, 268 D microscope (São Paulo, Brazil) coupled to an energy-dispersive X-ray spectroscopy (EDS) device operating at 100 kV. Samples for TEM were prepared by drop casting an isopropanol suspension of the samples over a carbon-coated copper grid, scanning electron microscopy (SEM) images were obtained with a LEO electron 440i microscope (Recife, Brazil) coupled to an EDS device operating at 30 kV. Samples were prepared over a carbon-coated copper grid and dried under ambient conditions.

Catalytic test

Glycerol oxidation was performed at 60-80 °C using a glass reactor Fischer-Porter (30 mL capacity). The glycerol solution (10 mL, 0.2 mol L^{-1} and NaOH/glycerol ratio = 4 mol/mol) was added into the reactor and the desired amount of catalyst (5.0% m/m) was suspended in the solution in an oxygen atmosphere under controlled pressure of 4 bar with time run 2-4 h. Samples were analyzed by high-performance chromatography (HPLC) using a Shimadzu LC20AT (city, country) performed with an AMINEX HPX-87H column (300 × 7.8 mm) with UV detection to analyze the mixture of the samples. H_3PO_4 0.1% solution was used as the eluent. The possible products were identified by comparison with the standard samples. The catalysis tests were also carried out on heat pre-treated catalysts.

After each use, the catalyst was removed from the reaction medium by magnetization, washed with distilled water at room temperature and dried in an oven at 100 °C for 12 h, then, the dried material was calcined in a muffle furnace at 600 °C for 2 h and reused.

Results and Discussion

The CF synthesis method by coprecipitation followed by calcination at 600 °C allowed the formation of crystalline nanoparticles with high magnetic coercivity (Hc = 510 kOe) and saturation magnetization (MS = 81.6 emu g^{-1}) that give the material suitable conditions for simple and quick recovery of the reaction medium by magnetization for reactivation and reuse in consecutive reaction cycles. The importance of its use as a support for bimetallic nanoparticles is linked to the possibility of recovering the material in a simple, fast and low operational cost so that the reaction product is free of catalyst residues in addition to facilitating the cleaning treatment for reuse in subsequent reaction cycles. The galvanic substitution process is relatively fast and, in the *ex situ* method, can be accompanied by a change in the color of the suspension of silver nanoparticles, which initially presents an intense yellow color and, with the addition of a palladium ion solution, it turns purple and then black at the end of the process depending on the palladium content added (Figure S1, Supplementary Information (SI) section). After the impregnation of the bimetallic NPs on the support and separation of the precipitate, the liquid phase presented a colorless appearance, qualitatively indicating the efficiency of the impregnation process of metallic nanoparticles to the magnetic support. Qualitative data were confirmed using X-ray fluorescence (XRF) assays (Table S1, SI section).

Using the XRF analysis data to study the chemical catalyst composition,it was possible to observe that CAP2 showed 20% replacement silver with palladium. The Co/Fe proportion corresponds to the stoichiometric relationship observed for the composition of cobalt ferrite and the silver-palladium content in relation to the support corresponds to 0.89%, a value very close to the theoretical value of 1.00% proposed for synthesis; this same observation applies to CAP4 (40% replacement of silver by palladium) and CAP8 (80% replacement).

As for bimetallic particles, for CAP2, the palladium content of 19.9% in relation to the total metal content is in accordance with the theoretical percentage proposed in the methodology. The CAP4 and CAP8 have a content of palladium in relation to the total metal content of 0.392 and 0.790 wt.%, respectively, reflecting the efficiency of the galvanic substitution process applied to the synthesis of bimetallic NPs. The higher content of palladium in the CAP catalyst demonstrates that the absence of support particles during the galvanic replacement process enabled a more efficient reaction than what was observed for other proposed methods such as the self-assembly or *in situ* method[37] in which the formation of nanoparticles occurs on the surface of the support.

The surface plasmon resonance (SPR) spectra of the suspension of Ag nanoparticles, Pd nanoparticles and Pd@Ag nanoparticles are shown in Figure 2. The nanoparticulate silver showed an intense and sharp absorption peak centered at 411 nm; Pd@Ag nanoparticles (Pd:Ag 40:60) in suspension showed a broad absorption peak at 437 nm. It can be seen from Figure 2 that the comparison of the spectra of the Pd@Ag and Ag nanoparticles reveals a redshift of the 26 nm bimetallic SPR peak. For palladium, no signal is observed in the region where the Ag and Pd-Ag absorption peaks appear. Li *et al.*[35] attribute this shift to a decrease in the electronic density of the Ag component in the bimetallic structure.

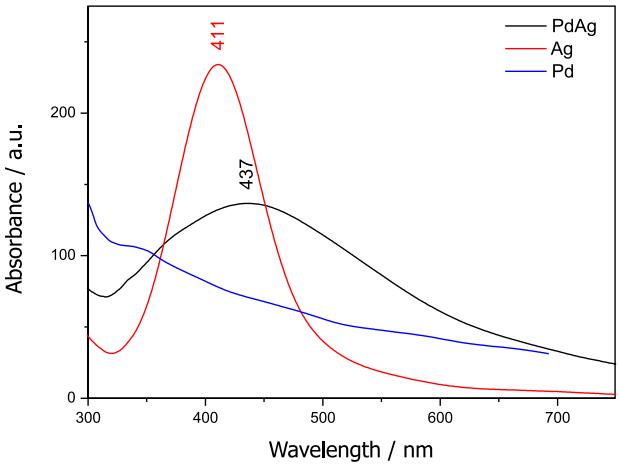

Figure 2. Comparative SPR spectra of Ag, Pd and Pd-Ag nanoparticles.

Based on the results presented by the catalytic tests, CAP4 was taken as a reference for the characterizations of the composite material produced. The TGA and DTA data (Figure 3) demonstrate that the CF undergoes a small mass loss of 5.2% in the temperature range from 27 to 183 °C attributed to the presence of adsorbed moisture on the surface of the material due to exposure to air in its stages of synthesis until packaging. In the range from 183 to 800 °C, the material did not show mass loss or thermal events characterized by alterations in the crystalline structure, demonstrating high thermal stability.

The CAP4 catalyst presents high thermal stability with a slight mass loss of 4.6% in the temperature range of 27 to 195 °C referring to moisture adsorbed on the surface of the solids. The values for the composite are close to those observed for the CF support after drying during the synthesis process. According to the data observed by thermogravimetric analysis, it was possible to define the calcination temperature of 600 °C as adequate for the production of the catalyst of uniform composition and free

of materials from the synthesis process and to use this same temperature for reactivation of the catalyst in the process of reuse, since at 600 °C it is possible to eliminate organic residues that would occupy the active sites on its surface and restore the same conditions as when it was first used.

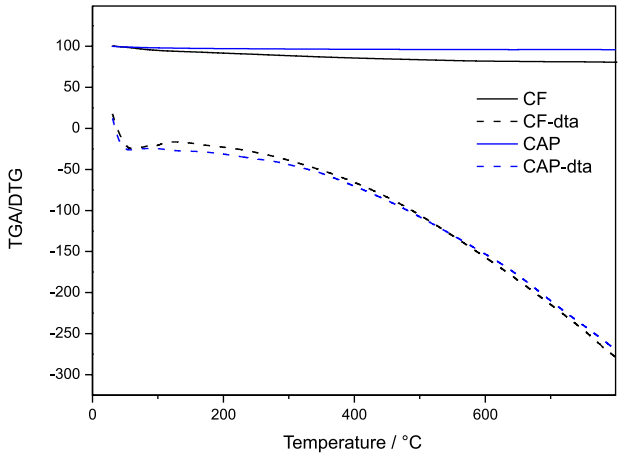

Figure 3. TGA and DTA curves of CF and CAP4 catalyst.

The XRD pattern of the as-synthesized $CoFe_2O_4$ nanoparticles is shown in Figure 4. An oxide of the inverse spinel-like structure was confirmed using the Joint Committee on Powder Diffraction Standard (JCPDS) crystallographic patterns, available at Crystallographica Search Match software.[38] The diffraction peaks correspond to the standard structure of $CoFe_2O_4$ (JCPDS card No. 22-1086). The pattern of the calcined $CoFe_2O_4$ visibly shows the formation of a high crystallinity phase. No other patterns were found on the $CoFe_2O_4$ sample, which demonstrates the efficiency of the co-precipitation method of synthesis. The determination of the crystallite size of CF powder is based on XRD line broadening and calculated using Debye-Scherrer's formula (equation 1).

$$D = K\lambda/\beta\cos\theta \quad (1)$$

In equation 1, D is the crystallite size (nm) of the phase under investigation, K is the Scherer's constant (0.9), λ is the X-ray wavelength of Cu Kα = 0.154 nm, β is the full-width at half maximum (FWHM) of the plane (311) and θ is the Bragg's angle. The calculated crystallite size of $CoFe_2O_4$ nanoparticles is found to be 52.65 nm.

The XRD pattern of the as-synthesized bimetallic silver-palladium nanoparticles coated CF (CAP4) using replacement galvanic process is shown in Figure 4. Two distinct diffraction peaks were observed at 2 values of 35.836 and 45.656, respectively, corresponding to the crystalline planes of cubic Ag (JCPDS cards 41-1402) and four distinct diffraction peaks were observed at 2 values of 27.612, 32.051, 45.656 and 56.623, respectively, corresponding to the crystalline planes of inorganic alloy COR PdO (JCPDS cards 46-1211) of electron diffraction pattern mixture of phases that include Pd metal. The XRD spectrum of palladium-silver coated CF (PdAg/$CoFe_2O_4$) reveals peaks of both the ferrite support and immobilized PdAg NPs. This spectrum confirms the support of bimetallic nanoparticles on the surface of cobalt ferrite nanoparticles. The crystallite size of CAP4 bimetallic nanoparticles as calculated by using XRD data, with no correction for instrumental broadening, is about 54.52 nm.

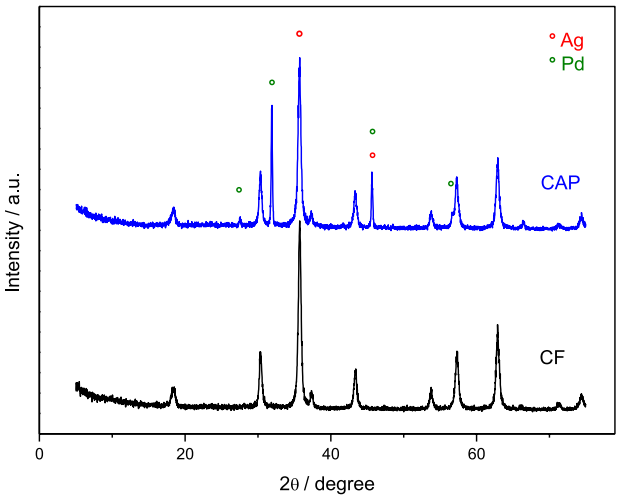

Figure 4. Diffractogram patterns of calcined CF and Pd-Ag/$CoFe_2O_4$.

The TEM images of the palladium-silver bimetallic nanoparticles are shown in Figure 5. The particles have an average size between 80 and 120 nm and oval morphology. The palladium particles (average size of 5 nm) are homogeneously distributed over the entire surface of the silver template, giving the material a wrinkled appearance. This surface dispersion structure of nanoparticles is extremely favorable to the catalytic action since the

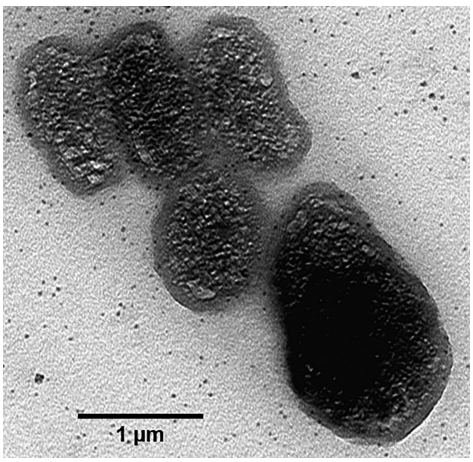

Figure 5. TEM image of palladium-silver nanoparticles.

entire contact area available for the catalyst has a similar composition.

SEM image of the catalyst is shown in Figure 6a. The catalyst particles have an irregular shape with a size of 40-80 nm and coalesced to each other forming aggregates with an average diameter of 1-3 μm due to the sintering effect provided by the heat treatment applied to the synthesis of the $CoFe_2O_4$ support. The EDX analysis of the catalyst (PdAg/$CoFe_2O_4$) shown in Figure 6b and Table S2 (SI section) showed that the distribution of the elements (atomic percentage) in the product was Co = 12.41%, Fe = 24.18% with iron/cobalt ratio in the nanoparticles of the catalyst by EDX found to be 1.95, which is very much close to the atomic ratio in the formula $CoFe_2O_4$.

The EDX data are in good agreement with the information obtained by XRF (Table S1). Pd@Ag NPs with palladium content of 0.790 wt.% provided the catalyst, in general terms, with a pronounced conversion and selectivity index for GALD much higher than the values observed for monometallic catalysts based on palladium,[10] silver[26] or bimetallic[39] with high silver content (Table 2).

The 0.20 mol L^{-1} glycerol solution and NaOH/glycerol ratio = 4 mol/mol were added into the reactor and the desired amount of catalyst (5.00 wt.%) was suspended in the solution in oxygen pressure (4 bar) controlled, temperature of 60-80 °C with time run 2-4 h. The conversion and selectivity were calculated using equations 2 and 3.

$$C\ (\%) = \Sigma A\ prod/(\Sigma A\ prod + A\ gly) \quad (2)$$

where ΣA prod represents the sum of the integrated area of the reaction products obtained from the chromatogram and ΣA gly represents the integrated area of glycerol.

$$S\ (\%) = Ax/\Sigma A\ prod \quad (3)$$

where Ax represents the integrated area of each product obtained from the chromatogram and ΣA prod represents the sum of the integrated area of the reaction products.

The catalytic performance of Ag/$CoFe_2O_4$ (ACF) and Pd/$CoFe_2O_4$ (PCF) monometallic was evaluated in the conversion of glycerol to GALD (Table 1). The maximum conversion of glycerol to the monometallic catalyst based on silver nanoparticles (ACF) was 6.05% with a reaction time of 4 h at a temperature of 80 °C and oxygen gas pressure of 4 bar. The formation of 30.41% GALD and 69.59% GLYA also shows that silver nanoparticles have low selectivity in the GLY oxidation process. In contrast, the catalyst based on palladium nanoparticles (PCF) exhibited a higher conversion than ACF under the same reaction conditions (17.01%) leading to the formation of glyceraldehyde (99.80%). Under milder conditions (at 60 °C), PCF presents a GLY conversion of 6.30%, which is very close to the yield of the oxidation reaction using the catalyst based on silver NPs in more energetic conditions, but with the advantage of presenting high selectivity.

Ag NPs demonstrate that they are more active than Pd NPs under the carbonyl oxidation mechanism of GALD, leading to the formation of the carboxyl group of GLYA, leading to the formation of a new product and thus reducing the selectivity of the process.

Griffin *et al.*[40] demonstrate that Pd/C and Au-Pd/C NPs have a greater tendency to form glycolate and lactate in oxidation reactions of ethylene glycol and 1,2-propanediol than the Au/C catalyst (tends to form acetate in typical carbonyl group reactions). The glycolate production reactions are typical of hydroxyl groups that, for the oxidation of GLY, lead to the formation of GALD with high selectivity using the CAP4 catalyst (Table 1). Xue *et al.*[41] investigated oxidation of 1,2-propanediol using of Pd-Ag bimetallic nanoparticles. The 1,2-propanediol conversion of 82.7% at the lactic acid selectivity was 92.8%. The

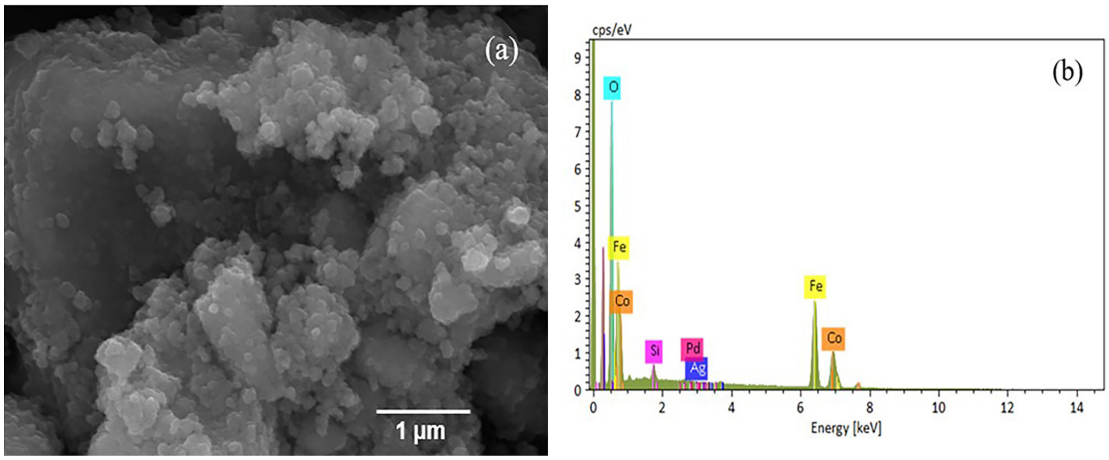

Figure 6. SEM with EDX of PdAg/$CoFe_2O_4$ catalyst.

Table 1. Conversion and selectivity of glycerol oxidation in run 1

Catalyst	Temperature / °C	time / h	Conversion / %	Selectivity / %			
				GALD	GLYA	TART	MESO
CAP4	80	4	57.00 ± 1.41	64.27 ± 2.25	28.16 ± 1.04	4.33 ± 0.57	2.21 ± 0.15
		2	52.77 ± 1.42	80.34 ± 2.51	19.12 ± 0.82	1.53 ± 0.50	–
	60	4	51.27 ± 1.67	88.32 ± 2.07	8.22 ± 1.07	2.44 ± 0.50	–
		2	49.07 ± 0.71	99.35 ± 0.31	0.23 ± 0.20	0.55 ± 0.15	–
ACF	80	4	6.05 ± 0.90	30.41 ± 0.40	69.59 ± 0.40	–	–
	60	4	4.59 ± 0.90	9.08 ± 0.40	90.91 ± 0.40	–	–
PCF	80	4	17.00 ± 0.90	99.80 ± 0.20	–	–	–
	60	4	6.30 ± 0.90	99.80 ± 0.20	–	–	–
CF	80	4	4.00 ± 0.50	–	–	–	–
	60	4	2.00 ± 0.50	–	–	–	–

GALD: glyceraldehyde; GLYA: glyceric acid; TART: tartronic acid; MESO: mesoxalic acid; CAP4: PdAg/$CoFe_2O_4$; ACF: Ag/$CoFe_2O_4$; PCF: Pd/$CoFe_2O_4$; CF: $CoFe_2O_4$.

selectivity for the carbonyl product (hydroxyacetone) of 1,2-propanediol oxidation was 2.7-7.8%, in addition to the formation of formic acid and acetic acid. Feng *et al.*[2] reported on their work the oxidation of 1,2-propanediol using hydroxyapatite (HAP) supported Pd and Pd-Ag catalysts prepared by the sol-immobilization method, and the formation of lactic acid as the main product of oxidation without the formation of significant amounts of hydroxyacetone. This reinforces the conclusions that silver nanoparticles have a great tendency to oxidize carbonyl groups of the initial product of the oxidation of alcohols, such as ethylene glycol, 1,2-propanediol and GLY, leading to the formation of acid carboxyls and thus decreasing the process selectivity. Table 2 presents the results of recent research on selective oxidation of GLY and we can observe the general trend of selectivity of silver NPs for carboxylic compounds.[13,42]

The synergistic effect of the formation of Pd@Ag NPs evidenced by UV-Vis spectrophotometry analysis (Figure 2) is directly related to the catalytic performance of bimetallic particles; CAP4 achieved yield twice as high as monometallic catalysts (57.00%) under the same reaction conditions. The selectivity of 64.27% for GALD shows that bimetallic nanoparticles are more active in the carbonyl oxidation process and the results observed for the reaction at 80 °C and 4 h of reaction confirm that higher temperatures or longer reaction time would lead to the formation of greater quantities of other by-products such as TART and MESO.

The catalysts based on silver-palladium NPs exhibit a high selectivity to GALD and GLYA and a conversion potential of 52.77% under reaction conditions of 60 °C, oxygen pressure of 4 bar, molar ratio NaOH/GLY = 4 in a reaction time of 2 h. The catalyst, acting at 80 °C for 4 h, showed a conversion of 57.00% and selectivity of 64.27% for GALD; the best reaction conditions were observed at 60 °C with a reaction time of 2 h (99.35% selectivity for GALD).

At the same temperature, the increase in the reaction time does not have a significant effect on the conversion but leads to a reduction in the selectivity to GALD for 88.32% due to the oxidation of this product and the formation of GLYA and TART. At 80 °C, it was not observe a significant increase in conversion but the oxidative potential of the catalyst was more pronounced since high percentages of GLYA (GALD oxidation product) were observed, with the formation of TART and MESO when the reaction occurs at 80 °C for 4 h. These are products of the sequential oxidation of GLY, as shown in Figure 1, where it can be seen that raising the reaction temperature creates energetically favorable conditions for the oxidation of GLY and its products. A similar effect can be observed at 60 °C when increasing the reaction time to 4 h raises the degree of conversion by only 2.20% but reduces the selectivity of GALD from 99.35 to 88.32% due to oxidation to GLYA, whose selectivity increased from 0.23% (at 60 °C with 2 h of reaction) to 8.22% and TART from 0.55 to 2.44%. The CF support has a low conversion potential in a GLY oxidation reaction under the same reaction conditions applied to the catalyst formed by bimetallic particles.

Effect of catalyst loading

When the bimetallic CAP2 (20% Pd content) and CAP8 (20% Ag content) catalysts were used for the catalytic oxidation of GLY, the conversion was greater for CAP4 (57.00%) than for CAP2 (6.30%) and

Table 2. Conversion and selectivity of the glycerol oxidation over different catalytic systems and conditions

Catalyst	Reaction conditions	Conversion / %	Selectivity / %								Reference
			DHA	GALD	GLYA	GCOA	TART	FA	HYP	OXA	
Ag/Al_2O_3	3.6 wt.% Ag, 5.0 wt.% catal., 3 h, 60 °C, 5 bar	85.0	–	–	10.3	57.1	–	30.6	–	0.6	42
Ag/Al_2O_3	1.0 wt.% Ag, 5.0 catal., 2 h, 80 °C, 5 bar	27.8	–	–	22.9	41.3	4.3	–	–	–	13
Ag/ZnO	Ag 0.7 wt.%, 5.0 wt.% catal., 5 h, 60 °C, 6 atm.	inactive	–	–	–	–	–	–	–	–	43
AgAu/ZnO	AgAu 2.0, wt.%, 5.0 wt.% catal., 5 h, 60 °C, 6 atm	10.00	–	77.0	8.0	–	–	7.0	–	8.0	
Pd/HAP	1.0 wt.% Pd, 6.0 wt.% catal., 5 h, 80 °C, 1 MPa (10 bar)	59.30	–	–	90.1	5.1	–	4.2	–	–	10
Pd/C110[a]	0.5 mol/1 KOH, 0.5 mol/1 GLY, 0.05 V s^{-1}	1.00-4.00	–	–	–	–	–	–	–	–	44
Pd/C	2.0 wt.% metal, 5.0 wt.% catal, 4 h, 353 K (80 °C), 0.3 MPa (3 bar)	2.80	66.1	22.5	10.9	0.5	–	–	–	–	29
Pd-Ag/C		9.50	81.9	8.9	5.6	1.6	–	–	2.0	–	
Pd-Ag/SiO_2		4.90	86.6	8.0	2.7	1.2	–	–	1.4	–	
Pd-Ag/TiO_2		1.70	90.0	5.9	2.9	0.7	–	–	–	0.5	
$PdAg/Al_2O_3$		6.80	86.4	7.3	3.4	0.6	–	–	1.8	0.5	
Pd-Ag/ZrO_2		3.20	91.3	6.2	2.1	0.2	–	–	–	0.2	
Pd-Ag/CeO_2		0.30	82.3	4.1	5.9	3.4	–	–	–	4.3	
Ag-Pd/CeO_2	1.5 wt.% Ag-Pd, 5 h, 60 °C, 5 bar	37.10	–	–	25.8	44.9	4.1	24.8	–	–	38
Pd-Ag[a]	0.1 mol L^{-1} KOH, 0.1 mol L^{-1} GLY, 2h, 25 °C, 1 atm	30.39	29.4	3.34	5.22	0.34	0.20	–	–	4.90	45

[a]Electrocatalysis. C110: electrode consisted of carbon; GLY: glycerol; DHA: dihydroyacetone; GALD: glyceraldehyde; GLYA: glyceric acid; GCOA: glycolic acid; FA: formic acid; OXA: oxalic acid; TART: tartronic acid; HYP: hydroxypyruvic acid; HAP: hydroxyapatite.

CAP8 (4.60%) as shown in Figure 7. The results indicate a tendency for CAP2 and CAP8 catalysts to behave as monometallic catalysts, however, with a gradual evolution of catalytic activity from CAP2 (GLY conversion of 19.5%) demonstrating that the synergistic effect between the metals Ag and Pd has a great effect on the catalytic activity for GLY oxidation reactions but has not reached its maximum potential. The data show that the high palladium content in the CAP8 catalyst inhibits the catalytic activity (GLY conversion of 26.0%) for reasons similar to those that justify the low catalytic performance of CAP2. At 60 °C (Table S3, SI section) a similar trend is observed as discussed for tests at 80 °C; the CAP2 catalyst proved to be more active for oxidation reactions from GALD to GLYA with 79.24% GALD selectivity and 20.75% GLYA selectivity).

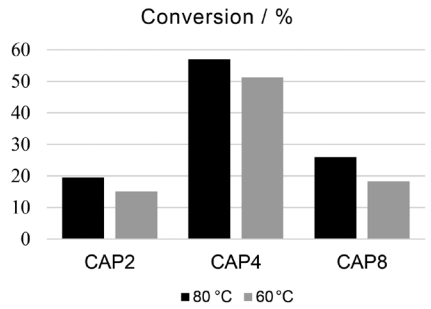

Figure 7. Glycerol conversion for the catalyst CAP2, CAP4 and CAP8. CAP2: PdAg/$CoFe_2O_4$ (20% Pd content); CAP4: PdAg/$CoFe_2O_4$ (40% Pd content); CAP8: PdAg/$CoFe_2O_4$ (80% Pd content).

The results proved that the coalesced Pd and Ag bimetallic nanoparticles in the catalyst synergistically catalyzed oxidation of GLY to GALD. The interaction (electrons transfer) between the coalesced Pd and Ag bimetallic nanoparticles in the catalyst probably played an important role in the catalytic oxidation reaction.

The catalyst was studied for 4 consecutive reaction cycles and its performance *per* cycle was evaluated to define its useful life. In Figure 8, it is possible to observe that at 80 °C with a reaction time of 4 h, there was a significant difference in the conversion percentage from the first cycle (57%) to the second cycle (53%) with the maintenance of the value for subsequent cycles (runs 3 and 4); a selectivity value difference outside the standard deviation is observed for GALD, 64% in the first cycle and 60% in the second cycle. Leaching effects caused by the high temperature and the longtime use of the catalyst may have altered its surface, causing a reduction in performance; the influence of the washing and reactivation process is ruled out since no significant reduction in conversion and selectivity is observed under soft reaction conditions with the application of the same methodology for catalyst reuse.

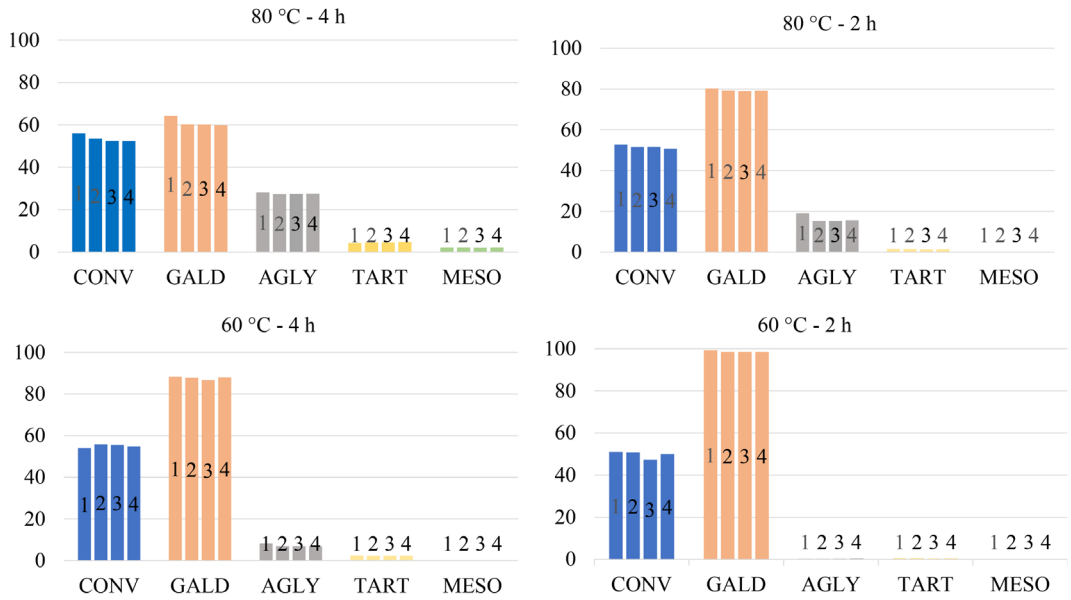

Figure 8. Recycling tests for the Ag-Pd/$CoFe_2O_4$ catalyst in glycerol oxidation reactions under optimized conditions. CONV: conversion; GALD: glyceraldehyde; GLYA: glyceric acid; TART: tartronic acid; MESO: mesoxalic acid.

Conclusions

The synthesis method of silver-palladium bimetallic nanoparticles by galvanic substitution proved to be simple, fast and relatively low cost for the formation of NPs with high conversion activity in GLY oxidation reactions and high selectivity for GALD. The Pd/Ag ratio is the defining factor of the catalytic activity and the *ex situ* method allows the formation of bimetallic NPs with a higher palladium content when compared with other synthesis methods and using the same theoretical proportions of reagents. The impregnation of NPs on cobalt ferrite was efficient and made the process of removing the catalyst from the reaction medium at the end of the process simple and practical. The reaction conditions studied can be considered mild and showed higher yields than those observed in studies published for other monometallic and bimetallic catalysts. The selectivity for GALD was not observed in any other published work, whether via selective oxidation, electrooxidation or biotechnological reaction strategies. The results show the possibility of applying bimetallic nanoparticles in other important oxidation reactions.

Supplementary Information

Supplementary information (Figure S1, Tables S1-S3) is available free of charge at http://jbcs.sbq.org.br as PDF file.

Acknowledgments

Technical support from the Interdisciplinary Laboratory of Advanced Materials (LIMAV); Northeast Strategic Technologies Center (CETENE); Analytical Instrumentation and Sample Preparation Group (GRIAPA) and the Diffraction and Fluorescence Laboratory of the Federal Institute of Education of Piaui (IFPI) are acknowledge.

Author Contributions

Milton S. Falcão was responsible for conceptualization, data curation, investigation, validation, writing (original draft, review and editing); Edmilson M. de Moura for conceptualization, project administration, formal analysis funding acquisition, investigation, resources, visualization, writing (original draft, review and editing); Jean C. S. Costa for data curation, software, writing (review and editing); Antonio F. A. A. Melo for data curation, writing (original draft, review and editing); Gilvan M. Paz for data curation, software, writing (review and editing); Ronaldo F. do Nascimento for data curation, software, writing (review and editing); Hélio O. do Nascimento for data curation, software, writing (review and editing); Luciano A. Montoro for data curation, software, writing (review and editing).

References

1. Chen, H.-Y.; Lu, J.; Fedeyko, J. M.; Raj, A.; *Appl. Catal., A* **2022**, *633*, 118534. [Crossref]
2. Feng, Y.; Xue, W.; Yin, H.; Meng, M.; Wang, A.; Liu, S.; *RSC Adv.* **2015**, *5*, 106918. [Crossref]
3. Hirasawa, S.; Nakagawa, Y.; Tomishige, K.; *Catal. Sci. Technol.* **2012**, *2*, 1150. [Crossref]

4. Torbina, V. V.; Vodyankin, A. A.; Ten, S.; Mamontov, G. V.; Salaev, M. A.; Sobolev, V. I.; Vodyankina, O. V.; *Catalysts* **2018**, *8*, 447. [Crossref]
5. Velázquez-Hernández, I.; Zamudio, E.; Rodríguez-Valadez, F. J.; García-Gómez, N. A.; Álvarez-Contreras, L.; Guerra-Balcázar, M.; Arjona, N.; *Fuel* **2020**, *262*, 116556. [Crossref]
6. Soufi, A.; Hajjoui, H.; Elmoubarki, R.; Abdennouri, M.; Qourzal, S.; Barka, N.; *Appl. Surf. Sci. Adv.* **2021**, *6*, 100145. [Crossref]
7. Hu, P.; Long, M.; *Appl. Catal., B* **2016**, *181*, 103. [Crossref]
8. Sahani, S.; Jaiswal, S.; Mishra, S.; Sharma, Y. C.; Han, S. S.; *Mol. Catal.* **2023**, *550*, 113508. [Crossref]
9. Rasrendra, C. B.; Culsum, N. T. U.; Rafiani, A.; Kadja, G. T. M.; *Bioresour. Technol. Rep.* **2023**, *23*, 101533. [Crossref]
10. Li, D.; Zhao, X.; Zhou, Q.; Ding, B.; Zheng, A.; Peng, Q.; Hou, Z.; *Green Energy Environ.* **2022**, *7*, 691. [Crossref]
11. Chen, J.; Wiley, B.; Mclellan, J.; Xiong, Y.; Li, Z.; Xia, Y.; *Nano Lett.* **2005**, *5*, 2058. [Crossref]
12. Wu, G.; Liu, Y.; He, Y.; Feng, J.; Li, D.; *Appl. Catal., B* **2021**, *291*, 120061. [Crossref]
13. Díaz, J. A.; Skrzyńska, E.; Zaid, S.; Girardon, J. S.; Capron, M.; Dumeignil, F.; Fongarland, P.; *J. Chem. Technol. Biotechnol.* **2017**, *92*, 2267. [Crossref]
14. Pestana, C. F. M.; Pinto, B. P.; Fernandes, D. R.; Mota, C. J. A.; *J. Braz. Chem. Soc.* **2022**, *33*, 1154. [Crossref]
15. de Assis, G. L.; Gonçalves, J. M.; Bernardes, J. S.; Araki, K.; *J. Braz. Chem. Soc.* **2020**, *31*, 2351. [Crossref]
16. Zhou, Y.; Shen, Y.; Xi, J.; Luo, X.; *ACS Appl. Mater. Interfaces* **2019**, *11*, 28953. [Crossref]
17. Bîtcan, I.; Petrovici, A.; Pellis, A.; Klébert, S.; Károly, Z.; Bereczki, L.; Péter, F.; Todea, A.; *Enzyme Microb. Technol.* **2023**, *163*, 110168. [Crossref]
18. Braun, M.; Santana, C. S.; Garcia, A. C.; Andronescu, C.; *Curr. Opin. Green Sustainable Chem.* **2023**, *41*, 100829. [Crossref]
19. Tang, D.; Lu, G.; Shen, Z.; Hu, Y.; Yao, L.; Li, B.; Zhao, G.; Peng, B.; Huang, X.; *J. Energy Chem.* **2023**, *77*, 80. [Crossref]
20. Luo, L.; Chen, W.; Xu, S.-M.; Yang, J.; Li, M.; Zhou, H.; Xu, M.; Shao, M.; Kong, X.; Li, Z.; Duan, H.; *J. Am. Chem. Soc.* **2022**, *144*, 7720. [Crossref]
21. Kolobova, N.; Pestryakov, N.; Bogdanchikova, N.; Cortés Corberán, V.; *Catal. Today* **2019**, *333*, 81. [Crossref]
22. de Abreu, W. C.; Garcia, M. A. S.; Nicolodi, S.; de Moura, C. V. R.; de Moura, E. M.; *RSC Adv.* **2018**, *8*, 3903. [Crossref]
23. Melo, I. E. M. S.; de Sousa, S. A. A.; Pereira, L. N. S.; Oliveira, J. M.; Castro, K. P. R.; Costa, J. C. S.; de Moura, E. M.; de Moura, C. V. R.; Garcia, M. A. S.; *ChemCatChem* **2019**, *11*, 3022. [Crossref]
24. Pereira, L. N. S.; Ribeiro, C. E. S.; Tofanello, A.; Costa, J. C. S.; de Moura, C. V. R.; Garcia, M. A. S.; de Moura, E. M.; *J. Braz. Chem. Soc.* **2019**, *30*, 1317. [Crossref]
25. Feng, Y.; Yin, H.; Wang, A.; Gao, D.; Zhu, X.; Shen, L.; Meng, M.; *Appl. Catal., A* **2014**, *482*, 49. [Crossref]
26. He, Z.; Ning, X.; Yang, G.; Wang, H.; Cao, Y.; Peng, F.; Yu, H.; *Catal. Today* **2020**, *365*, 162. [Crossref]
27. Liu, X.; Zou, Y.; Jiang, J.; *Appl. Catal., A* **2023**, *660*, 119216. [Crossref]
28. Ren, Z.; Li, Y.; Yu, L.; Wang, L.; Yang, Y.; Wei, M.; *Chem. Eng. J.* **2023**, *468*, 143623. [Crossref]
29. Hirasawa, S.; Watanabe, H.; Kizuka, T.; Nakagawa, Y.; Tomishige, K.; *J. Catal.* **2013**, *300*, 205. [Crossref]
30. Pakrieva, E.; Kolobova, E.; German, D.; Stucchi, M.; Villa, A.; Prati, L.; Carabineiro, S. A. C.; Bogdanchikova, N.; Corberán, V. C.; Pestryakov, A.; *Processes* **2020**, *8*, 1016. [Crossref]
31. Dodekatos, G.; Abis, L.; Freakley, S. J.; Tüysüz, H.; Hutchings, G. J.; *ChemCatChem* **2018**, *10*, 1351. [Crossref]
32. Falcão, M. S.; Garcia, M. A. S.; de Moura, C. V. R.; Nicolodi, S.; de Moura, E. M.; *J. Braz. Chem. Soc.* **2018**, *29*, 845. [Crossref]
33. Pereira, L. N. S.; Garcia, M. A. S.; Rozendo, J.; Vidinha, P.; Duarte, A.; de Moura, C. V. R.; de Moura, E. M.; *J. Braz. Chem. Soc.* **2020**, *31*, 1859. [Crossref]
34. Han, Y.; Gu, G.; Sun, J.; Wang, W.; Wan, H.; Xu, Z.; Zheng, S.; *Appl. Surf. Sci.* **2015**, *355*, 183. [Crossref]
35. Li, Y.; Liu, F.; Fan, Y.; Cheng, G.; Song, W.; Zhou, J.; *Appl. Surf. Sci.* **2018**, *462*, 207. [Crossref]
36. da Silva, A. G. M.; Rodrigues, T. S.; Slater, T. J. A.; Lewis, E. A.; Alves, R. S.; Fajardo, H. V.; Balzer, R.; da Silva, A. H. M.; de Freitas, I. C.; Oliveira, D. C.; Assaf, J. M.; Probst, L. F. D.; Haigh, S. J.; Camargo, P. H. C.; *ACS Appl. Mater. Interfaces* **2015**, *7*, 25624. [Crossref]
37. Stephanie, R.; Kim, M. W.; Kim, S. H.; Kim, J. K.; Park, C. Y.; Park, T. J.; *TrAC, Trends Anal. Chem.* **2021**, *135*, 116159. [Crossref]
38. *J. Appl. Cryst.* **1997**, *30*, 418. [Crossref]
39. Zaid, S.; Skrzyńska, E.; Addad, A.; Nandi, S.; Jalowiecki-Duhamel, L.; Girardon, J. S.; Capron, M.; Dumeignil, F.; *Top. Catal.* **2017**, *60*, 1072. [Crossref]
40. Griffin, M. B.; Rodriguez, A. A.; Montemore, M. M.; Monnier, J. R.; Williams, C. T.; Medlin, J. W.; *J. Catal.* **2013**, *307*, 111. [Crossref]
41. Xue, W.; Feng, Y.; Yin, H.; Liu, S.; Wang, A.; Shen, L.; *J. Nanosci. Nanotechnol.* **2016**, *16*, 9621. [Crossref]
42. Skrzyńska, E.; Zaid, S.; Addad, A.; Girardon, J. S.; Capron, M.; Dumeignil, F.; *Catal. Sci. Technol.* **2016**, *6*, 3182. [Crossref]
43. Kaskow, I.; Decyk, P.; Sobczak, I.; *Appl. Surf. Sci.* **2018**, *444*, 197. [Crossref]
44. Ivanov, R.; Nakova, A.; Tsakova, V.; *Electrochim. Acta* **2022**, *427*, 140871. [Crossref]
45. Yang, T.; Shen, Y.; *Langmuir* **2023**, *39*, 12855. [Crossref]

Submitted: November 20, 2023
Published online: January 16, 2024